Supplementary Material

Enhanced C2 and C3 Product Selectivity in electrochemical CO_2 Reduction on Carbon-doped Copper Oxide Catalysts prepared by Deep Eutectic Solvent Calcination

Melanie Iwanow, Johannes Seidler, Luciana Vieira, Manuela Kaiser, Daniel Van Opdenbosch, Cordt Zollfrank, Tobias Gärtner, Michael Richter, Burkhard König and Volker Sieber

Calculation of the crystallite size

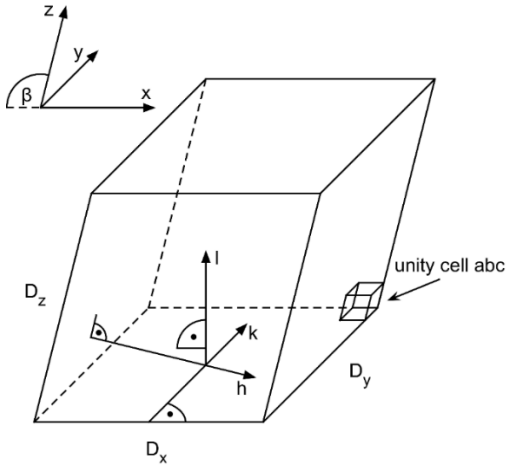

Figure S1. Scheme of the monoclinic CuO crystallite. Axes *h*, *k* and *l* are orthogonal to the planes, spanned by unity cell axes *a*, *b* and *c*.

The Scherrer equation relates the crystallite size to the width at half maximum of the peaks in a diffractogram. Since each peak represents a certain symmetry plane of the crystal, the shape of the crystallite can be estimated by the calculation of the length in the different directions. Scherrer's equation yields crystallite dimension in the reciprocal space. These dimensions can be converted into the size in the real space.

Directions $\vec{h}$, $\vec{k}$ and $\vec{l}$ in the reciprocal space are orthogonal to the according planes, spanned by unity cell axes $\vec{a}$, $\vec{b}$ and $\vec{c}$:

$\vec{h} \sim \vec{b} \times \vec{c}$

$\vec{k} \sim \vec{a} \times \vec{c}$

$\vec{l} \sim \vec{a} \times \vec{b}$

Tenorite (CuO) shows a monoclinic crystal system with angles $\alpha = \gamma = 90°$ and $\beta = 99.5°$. [1] Our measurements match well with the tenorite structure of the crystallography open database (COD) ID 9016326 (space group C1c1 and unit cell with a = 4.6927, b = 3.4283 and

c = 5.1370). Therefore, the mentioned vectors $\vec{h}$ and $\vec{l}$ are not parallel to the *x*- and *z*-axis, respectively (Figure S1).

The according values D_h and D_l obtained by Scherrer's equation need to be corrected by the angle β, while D_k corresponds directly to the size in the *y*-direction:

$\vec{h} \nparallel \vec{x} \Rightarrow D_x = D_h \cdot sin(\beta)$

$\vec{k} \parallel \vec{y} \Rightarrow D_y = D_k$

$\vec{l} \nparallel \vec{z} \Rightarrow D_z = \frac{D_l}{sin(\beta)}$

SEM investigations

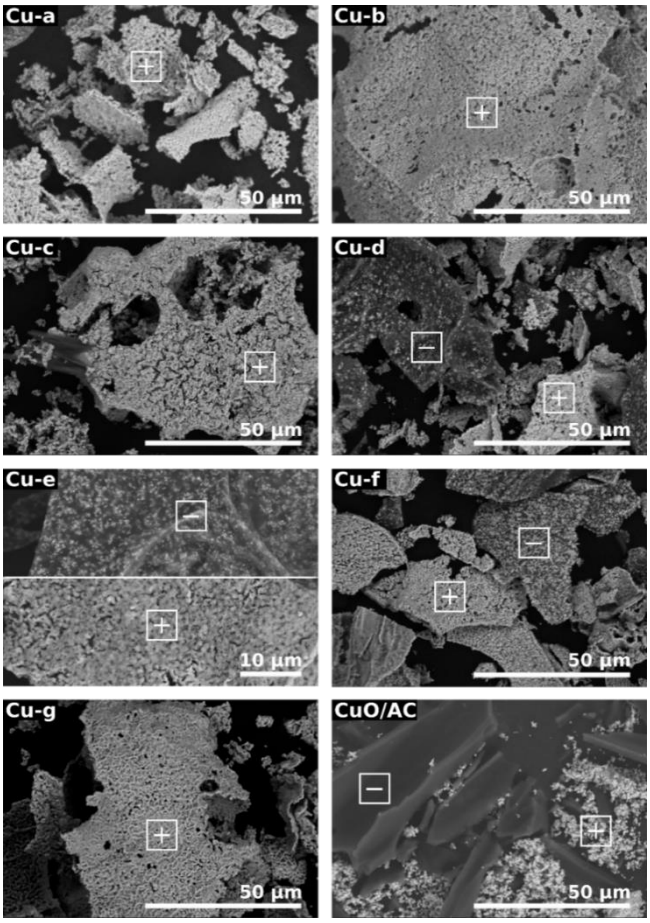

Figure S2. SEM images of synthesized copper materials comprising light (+) and dark (-) particle types. CuO/AC shows CuO mixed with activated carbon (commercial products).

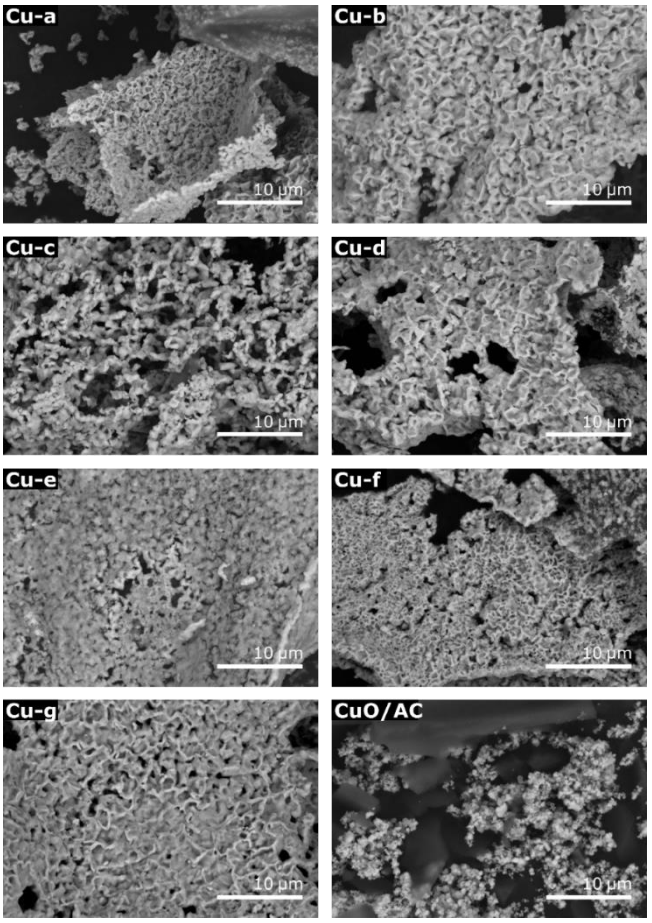

Figure S3. SEM images of all synthesized copper materials and CuO/AC.

XRD mesurements

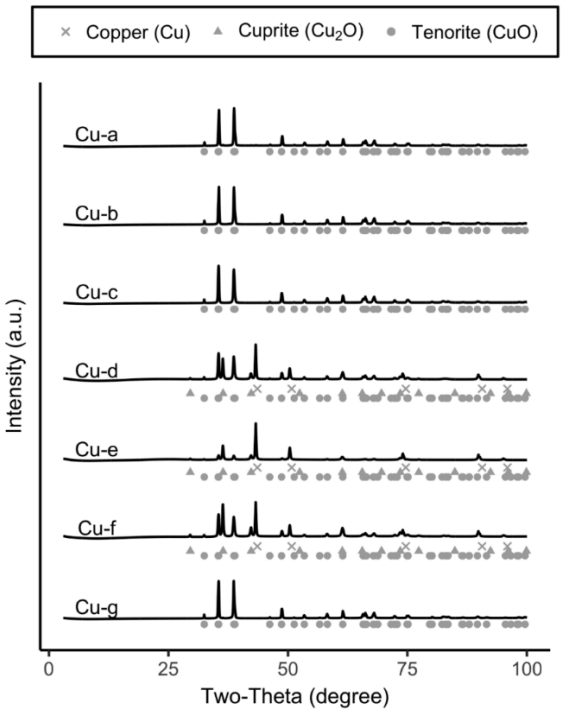

Figure S4. X-ray powder diffractograms of all copper catalysts show different copper oxidation states (0, +I and +II). The measurements are normalized to 1.

pH value

Table S1. Increase of pH during 2 h reaction time.

Catalyst	0 min	120 min
Cu-b	7.68	9.72
Cu-c	7.55	9.71
Cu-d	7.89	9.47
Cu-e	8.31	9.32
Cu-f	7.55	9.36
Cu-g	7.63	9.52
Cu-e, He-saturated	8.82	12.79

Optimization of electrochemical setup

Electrolyte concentration

Varying the electrolyte concentration affects the resulting current density and the selectivity of product formation.[2] Table S2 compares the catalyst activity in 0.1 M and 0.5 M $KHCO_3$ solutions. The formation rates of all products are higher in the concentrated 0.5 M $KHCO_3$ solution. Thus, following experiments were carried out with 0.5 M $KHCO_3$ electrolytes, since the product formation rates were higher and the electrochemical cell was more stable in this $KHCO_3$ concentrations.

Table S2. Total product formation rates for 2 h reaction time using copper catalyst Cu-a in two different concentrated $KHCO_3$ electrolytes at E = -1.7 V *vs.* Ag/AgCl.

$KHCO_3$ concentration [M]	Formation rates [µmol h^{-1} cm^{-2}]					
	H_2	CO	$HCOO^-$	C_2H_4	C_2H_5OH	C_3H_7OH
0.1	81.2	60.8	67.0	1.1	2.0	0.9
0.5	176.5	94.2	114.1	3.4	3.3	1.7

Catalyst loading and CO_2 gas flow

The effects of the catalyst loading on the gas diffusion layers and the CO_2 gas flow on product formation were investigated in 0.5 M $KHCO_3$. The product formation rate for Cu-a catalyst loadings of 5, 10 or 20 mg cm^{-2} for CO_2 gas flows of 5, 10 and 20 mL min^{-1} are shown in Figure S5. The variation of catalyst loading immobilized on a gas diffusion layer was investigated with a constant CO_2 gas flow of 5 mL min^{-1}. The catalyst amount influences distinctly formation rates of gaseous products. The highest hydrogen and carbon monoxide formation rates were achieved using a catalyst loading of 20 mg cm^{-2}, while ethylene shows higher formation rates on 5 mg cm^{-2}. Regarding liquid products (formate, ethanol and n-propanol), the catalyst loading shows less influence and a slight tendency towards a lower amount of catalyst was found. For example, ethanol formation rates of 3.5, 2.8 and 3.2 µmol h^{-1} cm^{-2} were obtained, when the catalyst loading was 5, 10 or 20 mg cm^{-2},

respectively. Thus, 5 mg cm^{-2} was chosen as the optimum of catalyst loading for this setup. This result is consistent to the findings of the optimum Cu/CNO catalyst amount by chronoamperometry measurements.[3]

The CO_2 gas flow, examined with 5 mg cm^{-2} of Cu-a, does not affect the product formation so significantly compared to the catalyst loading. At a higher gas flow of 20 mL min^{-1}, the formation rate of carbon monoxide increases, by a simultaneous decrease of ethylene formation. The electrochemical process was rather stable with a CO_2 gas flow of 10 mL min^{-1}, while the fluctuation for all products is high with 5 mL min^{-1}. This is in accordance to findings in literature that a higher CO_2 pressure favors the product formation from electrochemical CO_2 reduction.[4] Summarizing the experiments with benchmark catalyst Cu-a, gas diffusion layers coated with a lower catalyst loading (5 mg cm^{-2}), a CO_2 gas flow of 10 mL min^{-1} and more concentrated electrolytes (0.5 M) led to higher product formation rates and better stabilities of the electrochemical CO_2 reduction. Thus, these parameters were used for all following experiments.

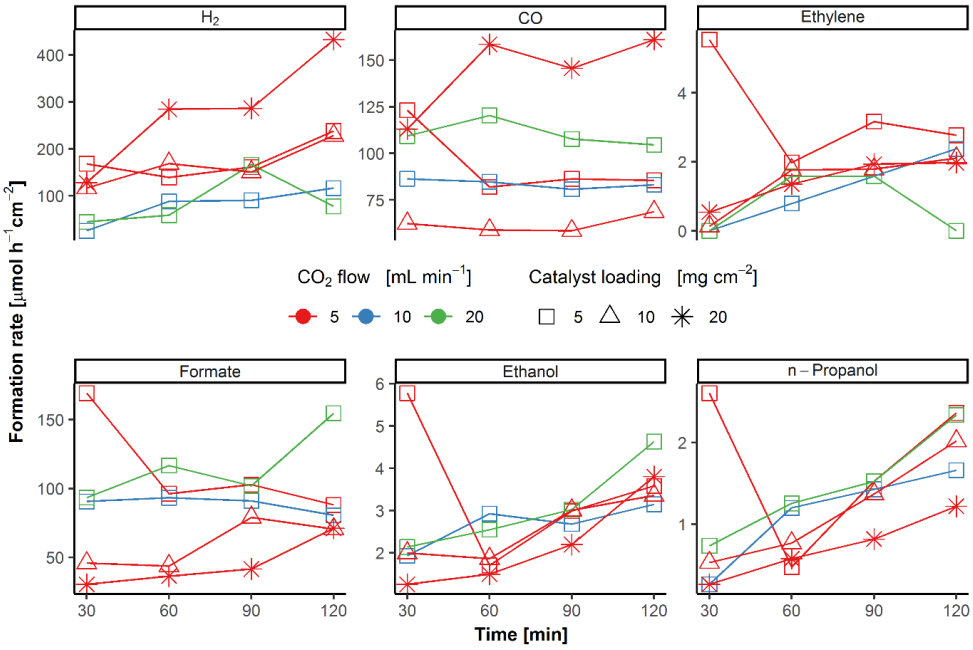

Figure S5. Formation rate of hydrogen, carbon monoxide, ethylene, formate, ethanol and n-propanol for different CO_2 flows and Cu-a catalyst loadings for two hours. The experiments were performed at constant potential *E* = - 1.7 V *vs.* Ag/AgCl in CO_2 saturated 0.5 M $KHCO_3$.

Potential

Using the above-mentioned parameters, the applied potential was varied between -2.1 V and -1.5 V *vs.* Ag/AgCl exemplarily for catalyst Cu-g. Faraday efficiency (FE) for the detected products shown along with the average current density at each step potential is illustrated in Figure S6. Carbon monoxide is produced at all potentials with FE between 6.3 % and 10.8 %. Stepping to more negative potentials from -1.9 V to -2.1 V increases the ethylene formation

from 5.9 % to 8.8 %, and decreases the efficiency of formate from 11.6 % to 10.9 %. The FE of ethanol and n-propanol is the highest at -1.7 V with 4.7 % (EtOH) and 5.5 % (n-PrOH). At this potential, the overall efficiency of hydrocarbons was also the highest with 40.9 % FE. Since the highest concentration of hydrocarbons was found at -1.7 V vs. Ag/AgCl, this potential was used for all further experiments.

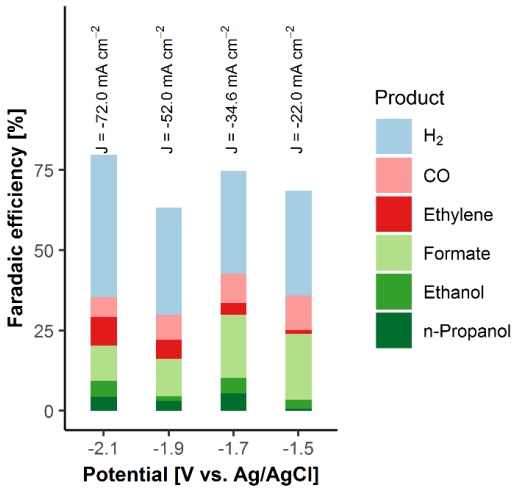

Figure S6. Products generated by the copper catalyst Cu-g between -2.1 V, -1.9 V, -1.7 V and -1.5 V in CO_2 saturated 0.5 M $KHCO_3$ electrolyte. The measurements were performed for half an hour at each potential.

Anolyte leaching

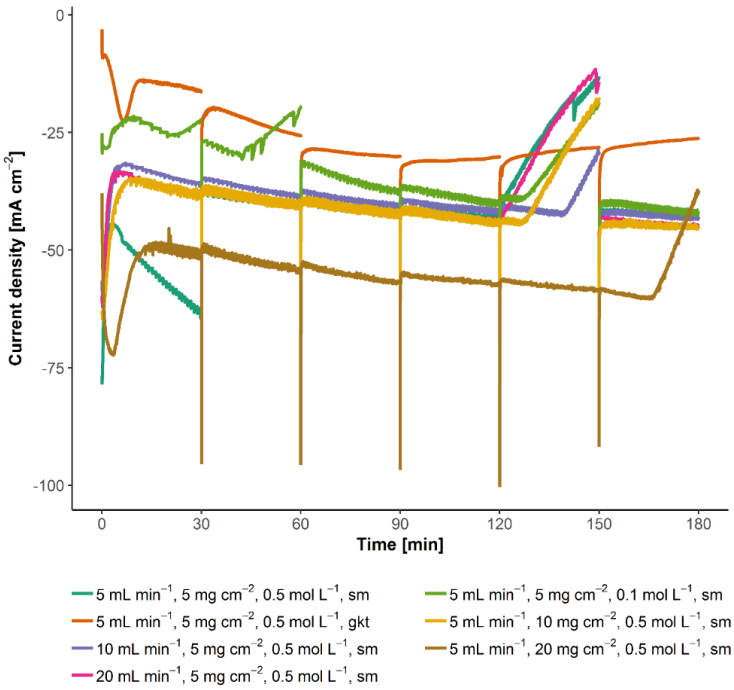

Figure S7. Overview of the current densities at -1.7 V *vs.* Ag/AgCl. The 0.1 M concentrated electrolyte degrades after ~ 40 min, while the 0.5 M $KHCO_3$ is stable for about 120 min.

Chronoamperometry

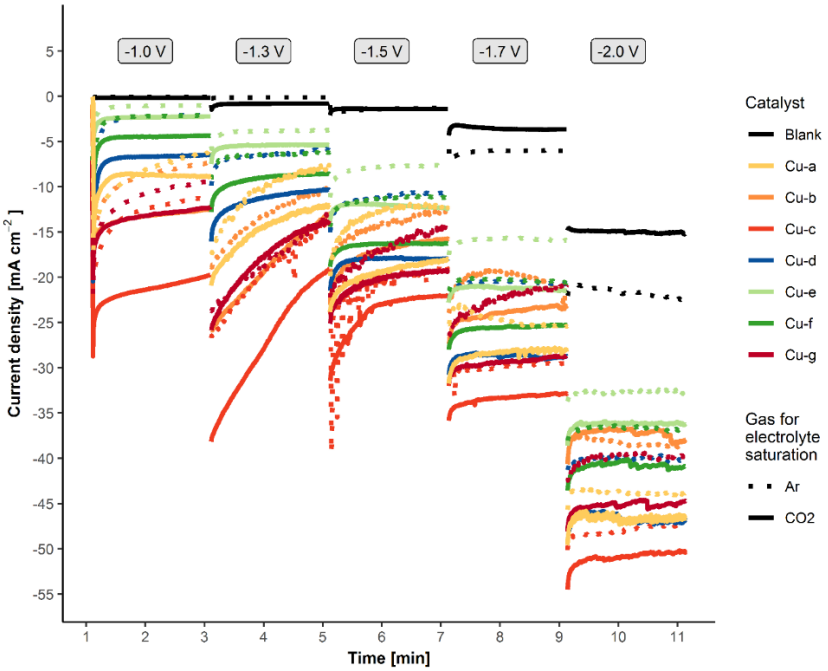

Figure S8. Chronoamperograms for synthesized copper catalysts in Argon and CO_2 saturated 0.5 M $KHCO_3$. Potentials shown vs. Ag/AgCl.

Faraday efficieny

Table S3. Faraday efficiencies of all synthesized copper materials at *E* = -1.7 V *vs.* Ag/AgCl in CO_2 saturated 0.5 M $KHCO_3$. In this table more detailed information of Figure 4b is shown.

Catalyst	FE [%]							J [mA cm^{-2}]
	total	H_2	CO	formate	ethylene	ethanol	n-propanol	
Cu-a	41.8	11.3	11.8	12.6	1.0	3.1	2.0	-41.75
Cu-b	70.5	26.1	7.4	17.5	7.7	5.3	6.4	-43.11
Cu-c	86.1	57.3	7.0	13.9	2.1	2.6	3.2	-35.79
Cu-d	70.3	54.4	6.4	8.8	—	0.4	0.3	-46.91
Cu-e	71.0	50.0	10.5	9.6	—	0.5	0.4	-33.25
Cu-f	65.3	54.5	4.0	6.6	—	0.1	—	-39.73
Cu-g	60.8	16.8	14.2	18.2	3.8	3.7	4.0	-35.70

[1] G. Tunell, E. Posnjak, C. J. Ksanda, in *Zeitschrift für Kristallographie - Crystalline Materials, Vol. 90*, **1935**, p. 120.

[2] A. S. Varela, M. Kroschel, T. Reier, P. Strasser, *Catalysis Today* **2016**, *260*, 8-13.

[3] M. Iwanow, L. Vieira, I. Rud, J. Seidler, M. Kaiser, D. Van Opdenbosch, C. Zollfrank, M. Richter, T. Gärtner, B. König, V. Sieber, *ChemistrySelect* **2020**, *5*, 11714-11720.

[4] a) O. Scialdone, A. Galia, G. L. Nero, F. Proietto, S. Sabatino, B. Schiavo, *Electrochimica Acta* **2016**, *199*, 332-341; b) Q. Lu, F. Jiao, *Nano Energy* **2016**, *29*, 439-456.